applied sciences

MDPI

Article

Numerical Experiment and Design of a Two-Rod Crank Knee Press with an Internal Layout of the Motor Drive

Amandyk Tuleshov [1,2], Balzhan Akhmetova [1,*], Moldir Kuatova [1,2], Bakhyt Merkibayeva [1,2] and Gulama-Garip Alisher Ibrayev [1]

[1] Joldasbekov Institute of Mechanics and Engineering, 050010 Almaty, Kazakhstan; aman_58@mail.ru (A.T.); kuatova.moldyr@mail.ru (M.K.); bakhyta23@mail.ru (B.M.); ybraev.alysher@mail.ru (G.-G.A.I.)
[2] Department of Mechanics, Al-Farabi Kazakh National University, 050010 Almaty, Kazakhstan
* Correspondence: balzhanibragimovna@mail.ru; Tel.: +7(775)0696862

Abstract: In crank presses, an important role is played by the presence of actuators with dwell, in which, with continuous movement of the input links, the output working link remains stationary at some part of the work. The use of a high-class structural group (fourth class) expands the functionality of the crank press, including it can ensure the link dwell of the working link on a given section of movement during the required period of time. As a result of the conducted numerical research, four variants of actuators of the crank knee press were designed. Due to the rational choice of the positions of racks and crosshead guide, the best layout of the dimensions of the press mechanism has been achieved. Changing the coordinates of the racks accordingly allows for designing a mechanism with upper or lower dwells of the working links. The duration of the dwell of the working link (slider) can be adjusted by selecting the distance between the racks with rotational pairs and a crosshead guide of the mechanism. All this is shown on the basis of a numerical experiment based on kinematic analysis. In addition, the proposed structure of the mechanism makes it possible to ensure the exact link dwell, which cannot be achieved due to the well-known knee presses based on the second-class mechanism.

Keywords: crank knee press; double-rod press; high-class mechanisms; output link dwell; numerical experiment; crank press design

check for updates

Citation: Tuleshov, A.; Akhmetova, B.; Kuatova, M.; Merkibayeva, B.; Ibrayev, G.-G.A. Numerical Experiment and Design of a Two-Rod Crank Knee Press with an Internal Layout of the Motor Drive. *Appl. Sci.* **2023**, *13*, 10948. https://doi.org/10.3390/app131910948

Academic Editor: Angelo Luongo

Received: 12 August 2023
Revised: 25 September 2023
Accepted: 26 September 2023
Published: 3 October 2023

Copyright: © 2023 by the authors. Licensee MDPI, Basel, Switzerland. This article is an open access article distributed under the terms and conditions of the Creative Commons Attribution (CC BY) license (https://creativecommons.org/licenses/by/4.0/).

1. Introduction and Review of Sources

The study and expansion of the functional capabilities of crank-slide actuating mechanisms based on four-link structural groups is attractive for the development of new designs of crank presses and other stamping and forging machines [1,2]. They eliminate such disadvantages of existing crank presses as the distortion of the working slider in the process of forging compression and the limitations of the design for the implementation of the working slider dwells [1,3,4].

One of the most important characteristics of the press is the rigidity of its structural elements [1,5]. The rigidity of the press significantly affects the duration of the loading and unloading phases: the greater the rigidity of the links, the shorter the contact time of the stamp with the forging. This is especially important for increasing the stability of stamps in hot stamping processes [3,5]. However, an increase in the rigidity of the press structure leads to an increase in its metal consumption, which is not always economically feasible. Therefore, for example, for a number of technological operations, in particular, to improve the quality of forging during cold stamping, it is desirable, on the contrary, to increase the duration of contact of the stamp with the workpiece [4].

Long-term contact of the stamp with the workpiece is ensured due to the operating link dwell. The four-link crank-slider mechanism cannot provide a long-term dwell of the working slider [1]. For this purpose, six-link mechanisms are used, which are obtained by layering a two-link group to a four-link crank-slider kinematic chain. Thus, a crank-knee mechanism is obtained, allowing the working slider dwell [6].

The crank-slider six-link mechanism is used as a feed mechanism for cutting a rubber with a circular saw [7]. In the work [8], crank press made of a single-circuit five-link linkage with two degrees of freedom (2 DOF) has a drive with an adjustable electric motor of alternating current (AC). Dual-circuit hybrid crank presses with two degrees of freedom (2 DOF) are designed on the basis of seven-link lever mechanisms [9,10]. Hybrid presses use two engines, one of which "simulates" an AC-engine, prescribing a trajectory profile with a constant speed. The other allows for programming the cyclogram of the technological process by controlling the servo motor.

In the works [11,12] a crank-slide double-rod mechanism of Stephenson II is proposed, which, in comparison with the existing operating mechanism of the crank press, has broader functionality. The structure of such mechanisms makes it possible to realize the exact working link dwell [13].

In work [14], studies were conducted on the synthesis of hybrid mechanisms with five rods using genetic algorithms. A study was conducted [15] on modeling and kinematic analysis of a hybrid drive of a seven-stage mechanism with an adjustable crank. In work [16], a study was conducted using a hybrid machine (HM) system with a five-girder mechanism. In work [17], a configuration of seven rods was applied using kinematic analysis and optimal design of a hybrid system. In work [18], a seven-stage mechanism was presented, which was later used to study the efficiency of stamping and energy distribution between a servo motor and a flywheel with different motion inputs. In addition, ref. [19] has also developed a control system for the seven-stage mechanism using iterative learning management and feedback control methods. Yang and Chen proposed a knee press configuration to approximate a dwell motion, involving additional cranks and connecting rods for force transmission, potentially increasing the design and manufacturing complexity [20]. In [21], authors present the development of a single-degree-of-freedom eight-bar planar mechanism designed to improve precision and dwell motion in industrial applications, utilizing slider balance and optimization techniques for reduced manufacturing complexity and cost.

This paper investigates an eight-link crank knee press with an internal engine arrangement for the first time, as shown in Figure 1. The press mechanism consists of a frame O and Q, a crank 1, a rocker arm 3, a three-hinged link 4, and a slider 7. The slider 7 has two hinges E and D, with which connecting rods 5 and 6 are connected, respectively. Three-pair link 4, connecting rods 5, 6 and slider 7 form a four-link variable closed loop EDCF. The connecting rod 6 in hinge B is connected to the crank 1 by means of a link 2.

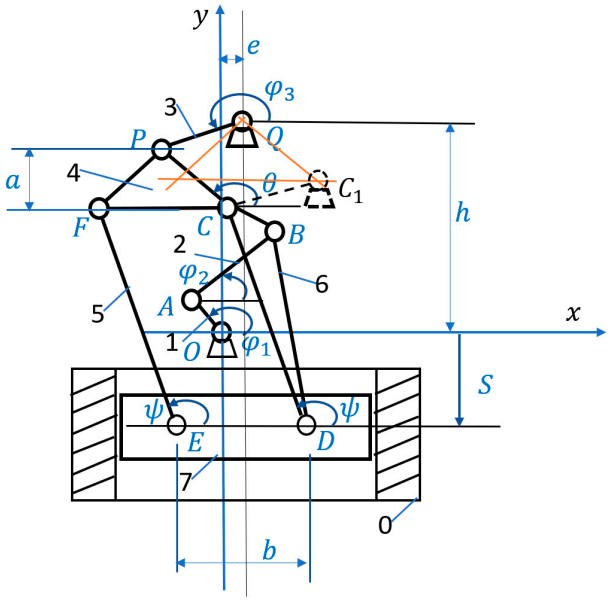


Figure 1. Kinematic diagram of an eight—link crank knee press with an internal engine location.

The research aims to illustrate the functionality of the knee press actuator through a numerical experiment. The practical significance of the study lies in its ability to demonstrate how such an actuator arrangement reduces the external dimensions of the crank press and improves the transmission of forces from the crank to the working slider in comparison with the mechanism described in [12]. The investigation involves a numerical experiment on the kinematics of this mechanism structure to explore its functionality and derive the geometric dimensions necessary for prolonged slider dwell times. Additionally, a method for studying the kinematics of the eight-link crank knee press with the internal engine arrangement is proposed.

2. Kinematic Analysis

The kinematic scheme of a two-rod crank knee press with an internal engine arrangement is shown in Figure 1. The mechanism under consideration has the following design features: (a) between the lengths of the links there is an equality $|ED| = |FC|$, $|CD| = |FE|$, $|FP| = |CP|$; (b) link 4 makes a forward motion [1], therefore $\theta = const$, also there is $\varphi_6 = \varphi_5 = \psi$. Another feature of this mechanism structure is that the coordinates of the frame Q lies on the straight line of the stroke of the working slider 7.

Based on the kinematic scheme of the mechanism, we write down the equations in vector form:

$$\begin{gathered}\vec{OA} + \vec{AB} + \vec{BC} + \vec{CP} = \vec{h} + \vec{e} + \vec{QP}, \\ \vec{h} + \vec{e} + \vec{QP} = \vec{S} + \vec{e} + \tfrac{1}{2}\vec{b} + \vec{DC} + \vec{CP}.\end{gathered} \tag{1}$$

We introduce the following labeling $l_1 = |AO|$, $l_2 = |AB|$, $l_{BC} = |BC|$, $l_{CP} = |CP|$, $l_3 = |PQ|$, $l_6 = |DC|$, $l_5 = |EF|$, $l_{CP} = |CP|$, $\alpha_6 = \measuredangle DCB = const$, $\varphi_{BC} = \psi + \alpha_6$. Taking into account the adopted labeling, the projections of Equation (1) on the coordinate axes are written as follows:

$$\begin{gathered}l_1\cos\varphi_1 + l_2\cos\varphi_2 + l_{BC}\cos(\psi + \alpha_6) + l_{CP}\cos\theta = l_3\cos\varphi_3 + e \\ l_1\sin\varphi_1 + l_2\sin\varphi_2 + l_{BC}\sin(\psi + \alpha_6) + l_{CP}\sin\theta = l_3\sin\varphi_3 + h \\ l_3\cos\varphi_3 = \tfrac{1}{2}b + l_6\cos\psi + l_{CP}\cos\theta \\ h + l_3\sin\varphi_3 = S + l_6\sin\psi + l_{CP}\sin\theta\end{gathered} \tag{2}$$

System (2) will be written in the following form:

$$\begin{gathered}l_2\cos\varphi_2 + l_{BC}\cos(\psi + \alpha_6) - l_3\cos\varphi_3 = l_\beta\cos\beta \\ l_2\sin\varphi_2 + l_{BC}\sin(\psi + \alpha_6) - l_3\sin\varphi_3 = l_\beta\sin\beta \\ l_3\cos\varphi_3 - l_6\cos\psi = c \\ l_3\sin\varphi_3 - l_6\sin\psi - S = d\end{gathered} \tag{3}$$

where

$$\begin{gathered}l_\beta\cos\beta = e - l_{CP}\cos\theta - l_1\cos\varphi_1,\ \sin\beta = h - l_{CP}\sin\theta - l_1\sin\varphi_1 \\ c = \tfrac{1}{2}b + l_{CP}\cos\theta = const,\ d = -h + l_{CP}\sin\theta = const\end{gathered} \tag{4}$$

In the mechanism under consideration, the variable kinematic parameters are $\varphi_1, \varphi_2, \varphi_3, \psi, S$. It is assumed that the engine will be connected to link 1 and mounted on the frame O. Hence, the angular coordinate of the input link is taken as the generalized coordinate 1—φ_1. According to Artobolevsky [6], the mechanism belongs to the fourth class since the driven kinematic chain contains a four-sided closed loop and the structural group (2,3,4,5,6,7) does not break up into groups of a smaller order.

At the same time, the analysis of the positions of the mechanism for a given φ_1, i.e., system (3) has no analytical solutions. From the analysis of system (3), it can be seen that the first three equations of system (3) relative to φ_2, φ_3, ψ represent a system of nonlinear trigonometric equations, which should be solved by approximate numerical methods. Then, from the last equation of system (3), the coordinate of the slider is determined 7—S.

To construct an effective numerical algorithm for the kinematic analysis of the mechanism under consideration, we apply the following approach.

Based on system (3), we write the kinematics equations of the mechanism in small displacements [2] with respect to $\boldsymbol{\varphi_2}, \boldsymbol{\psi}, \boldsymbol{\varphi_3}$ in the form of a matrix equation (3 × 3):

$$A\vec{x} = \vec{b} \tag{5}$$

where $\vec{x} = \begin{bmatrix}\Delta\varphi_2 & \Delta\psi & \Delta\varphi_3\end{bmatrix}^T$, $\vec{b} = \begin{bmatrix}-l_1\Delta\varphi_1\sin\varphi_1 & -l_1\Delta\varphi_1\cos\varphi_1 & 0\end{bmatrix}^T$ and

$$A = \begin{bmatrix} l_2\sin\varphi_2 & l_{BC}\sin(\psi+\alpha_6) & -l_3\sin\varphi_3 \\ l_2\cos\varphi_2 & l_{BC}\cos(\psi+\alpha_6) & -l_3\cos\varphi_3 \\ 0 & l_6\sin\psi & -l_3\sin\varphi_3 \end{bmatrix} \tag{6}$$

The solution to system (5) has the following form:

$$\begin{aligned} \Delta\varphi_2 &= \frac{\Delta\varphi_1}{\lceil A\rceil_{det}} l_3 l_1 [l_{BC}\sin\varphi_3\sin(\psi+\alpha_6-\varphi_1) + l_6\sin\psi\sin(\varphi_3-\varphi_1)] \\ \Delta\psi &= \frac{\Delta\varphi_1}{\lceil A\rceil_{det}} l_3 l_2 l_1 \sin\varphi_3\sin(\varphi_2-\varphi_1) \\ \Delta\varphi_3 &= \frac{\Delta\varphi_1}{\lceil A\rceil_{det}} l_6 l_2 l_1 \sin\psi\sin(\varphi_2-\varphi_1) \end{aligned} \tag{7}$$

where

$$\lceil A\rceil_{det} = l_2 l_3 [l_{BC}\sin\varphi_3\sin(\psi+\alpha_6-\varphi_2) - l_6\sin\psi\sin(\varphi_3-\varphi_2)] \neq 0 \tag{8}$$

3. Analysis of Special Positions of the Mechanism

Analysis of special positions of the mechanism. When solving the system (7) in small movements, it is necessary to satisfy the condition (8), i.e., it is necessary to exclude special positions of the mechanism. A technique that allows for establishing special positions of the mechanism based on the analysis of the functional from equation is proposed (8):

$$F(\varphi_2, \varphi_3, \psi) = l_{BC}\sin\varphi_3\sin(\psi+\alpha_6-\varphi_2) - l_6\sin\psi\sin(\varphi_3-\varphi_2) = 0 \tag{9}$$

Let us consider a trivial solution to Equation (9) with geometric interpretation. Below are the options for these solutions:

(A) let $\sin\varphi_3 = 0$, then the Equation (9) is performed in two versions: (1) $\sin\psi = 0$ or (and) (2) $\sin(\varphi_3 - \varphi_2) = 0$. In the first version, we have at $\varphi_3 = 0$ **or** π result $\psi = 0$ **or** π; in the second version at $\varphi_3 = 0$ **or** π turns out $\varphi_3 = \varphi_2$. The first version is interpreted as follows: link ***QP*** and links ***CD***, ***FE*** occupy mutually parallel positions. In the second case links ***QP*** and ***AB*** are parallel.

(B) let $\sin(\psi + \alpha_6 - \varphi_2) = 0$, hence there is a $\varphi_2 = \psi + \alpha_6$ which happens when links ***AB*** and ***CB*** are parallel. For a trivial solution to Equation (9), one of two variants must also be fulfilled here: (3) $\sin\psi = 0$ or (and) (4) $\sin(\varphi_3 - \varphi_2) = 0$. In the third version the links ***CD***, ***FE*** occupy a perpendicular position relative to the slide stroke. In the fourth version the links ***QP*** and ***AB*** are parallel.

In order to visualize the functional (9) in a three-dimensional system, a fixed value of one the parameters should be set. Such parameter is ψ, which has the following domain of variability $\frac{\pi}{2} - tan^{-1}\frac{r}{l} \leq \psi \leq \frac{\pi}{2} + tan^{-1}\frac{r}{l}$, where r—crank length, *l*—rod length BC.

Further, for clarity the functional $F(\varphi_2, \varphi_3, \psi)$ is presented in Figure 2 at following values ψ = 1.8165; 1.7182; 1.6199; 1.5216; 1.3251 [rad] in the system of coordinates $\{F(\varphi_2, \varphi_3), \varphi_2, \varphi_3\}$. This case corresponds to a second version.

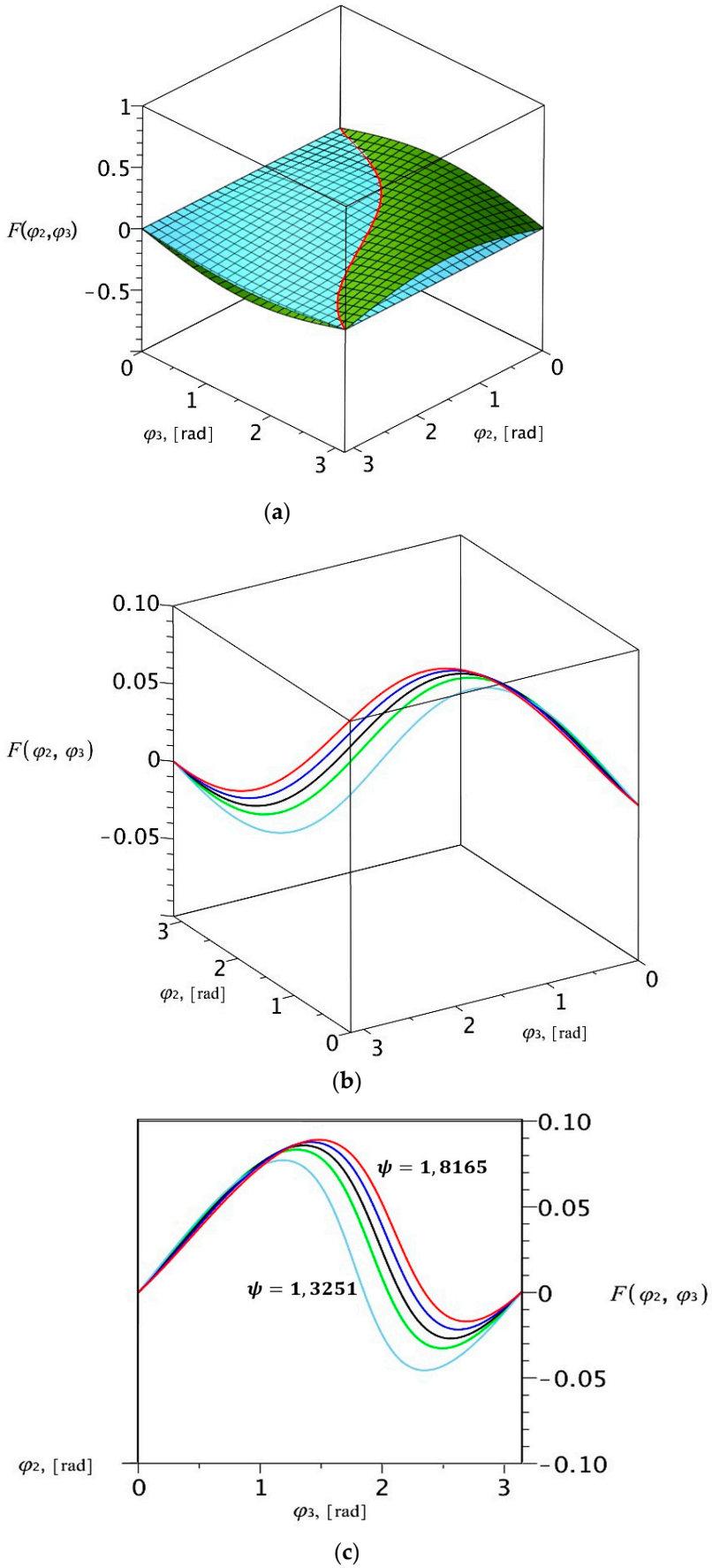


Figure 2. Functional graphs $\boldsymbol{F(\varphi_2, \varphi_3, \psi)}$ in the three-dimensional system $\{\boldsymbol{F(\varphi_2, \varphi_3), \varphi_2, \varphi_3}\}$.

Figure 2a shows the functional $F(\varphi_2, \varphi_3, \psi = const) = F_1 + F_2$. That is, with a fixed ψ = 1.8165 as the intersection of two functions $F_1 = l_{BC}\sin\varphi_3\sin(\psi + \alpha_6 - \varphi_2)$ and $F_2 = -l_6\sin\psi\sin(\varphi_3 - \varphi_2)$. Further built were F_1 and F_2 at other values ψ = **1.7182; 1.6199; 1.5216; 1.3251** [rad] which are shown in Figure 2b in the form of intersection curves of these two surfaces. In Figure 2c the intersection curves are projected on a plane $\{\varphi_2, F\}$. Thus, in Figure 2, the special position of the mechanism corresponds to $\varphi_3 = 0$ and $\varphi_2 = 0$ or $\varphi_3 = \pi$ and $\varphi_2 = \pi$.

4. Methods and Algorithms of Kinematic Analysis

The solution of system (7) is correct only in a certain assembly of the mechanism when the condition is met (8). Therefore, from the beginning it is necessary to select the assembly of the mechanism, and as a consequence, to set the initial values of the variable parameters on which the continuous movement of the mechanism is possible. The problem of determining the assembly and the initial position of the mechanism is solved by replacing the leading link [3], i.e., by choosing another variable as a generalized coordinate, which makes it possible to simplify the solution of the original system (2). This variable is called conditional generalized coordinate (CGC) [4].

The analysis of system (2) shows that it is advisable to take as CGC the angular coordinate φ_3. Considering this, the system (2) can be represented as the following:

$$\begin{gathered} l_1\cos\varphi_1 + l_2\cos\varphi_2 = l_3\cos\varphi_3 - l_{BC}\cos(\psi + \alpha_6) + p \\ l_1\sin\varphi_1 + l_2\sin\varphi_2 = l_3\sin\varphi_3 - l_{BC}\sin(\psi + \alpha_6) + r \\ l_6\cos\psi = l_3\cos\varphi_3 - c \end{gathered} \tag{10}$$

$$S + l_6\sin\psi = l_3\sin\varphi_3 + d \tag{11}$$

where $p = -l_{CP}\cos\theta + e, r = -l_{CP}\sin\theta + h$.

At a given coordinate φ_3 solutions of system (10) with respect to ψ, S, φ_2, φ_1 are represented as the following decisive algorithm 1:

[1]. Constant parameters are set and calculated: x_O, y_O, l_1, l_2, l_{BC}, l_{CP}, l_3, l_6, l_5, l_{CP}, α_6, θ, a, b, h, e, p, r, c, d;

[2]. $\psi^{(1,2)} = \mp\cos^{-1}\frac{(l_3\cos\varphi_3 - c)}{l_6}$;

[3]. $S = l_3\sin\varphi_3 - l_6\sin\psi + d$;

[4]. $\gamma = \tan^{-1}\frac{l_3\sin\varphi_3 - l_{BC}\sin(\psi+\alpha_6)+r}{l_3\cos\varphi_3 - l_{BC}\cos(\psi+\alpha_6)+p}$, given that $l_3\cos\varphi_3 \neq l_{BC}\cos(\psi + \alpha_6) + p$;

[5]. $l_\gamma = \sqrt{(l_3\cos\varphi_3 - l_{BC}\cos(\psi + \alpha_6) + p)^2 + (l_3\sin\varphi_3 - l_{BC}\sin(\psi + \alpha_6) + r)^2}$;

[6]. $\varphi_2^{(1,2)} = \gamma \pm \cos^{-1}\frac{l_1^2 + l_\gamma^2 - l_2^2}{2l_1l_\gamma}$;

$$\varphi_1^{(1,2)} = \gamma \pm \cos^{-1}\frac{l_2^2 + l_\gamma^2 - l_1^2}{2l_2l_\gamma} \tag{12}$$

Then the assembly of the mechanism is built. To do this, the equations of the coordinates of the hinges are used:

$$\begin{gathered} x_A = l_1\cos\varphi_1,\ y_A = l_1\sin\varphi_1 \\ x_B = l_1\cos\varphi_1 + l_2\cos\varphi_2 = x_A + l_2\cos\varphi_2, \\ y_B = l_1\sin\varphi_1 + l_2\sin\varphi_2 = y_A + l_2\sin\varphi_2, \end{gathered}$$

$$x_C = l_1\cos\varphi_1 + l_2\cos\varphi_2 + l_{BC}\cos(\psi + \alpha_6) = x_B + l_{BC}\cos(\psi + \alpha_6) \tag{13}$$

$$\begin{gathered} y_C = l_1\sin\varphi_1 + l_2\sin\varphi_2 + l_{BC}\sin(\psi + \alpha_6) = y_B + l_{BC}\sin(\psi + \alpha_6), \\ x_P = l_3\cos\varphi_3 + e,\ y_P = l_3\sin\varphi_3 + h, \\ x_F = l_3\cos\varphi_3 + e - \tfrac{b}{2} = x_P - \tfrac{b}{2},\ y_F = l_3\sin\varphi_3 + h - a = y_P - a, \\ x_E = x_F - l_6\cos\psi,\ y_E = y_F - l_6\sin\psi,\ x_D = x_E + b,\ y_D = y_E, \end{gathered}$$

and the mechanism leash equations

$$(x_j - x_i)^2 + (y_j - y_i)^2 = l_{ji}^2, \tag{14}$$

where indexes i, j are assumed to be equal to the numbers of the hinges in accordance with the schemes of the mechanism shown in Figure 3. At the same time, the following matches are between the letters (Figure 1) and digital (Figure 3) designations: $O-12$, $A-13$, $B-11$, $D-5$, $C-8$, $E-6$, $F-7$, $P-9$, $Q-10$, 14–15—indicates the crosshead guide.

Thus, on the basis of algorithm 1, assembly options and the choice of the desired assembly are established. The initial positions of the mechanism are determined at $\boldsymbol{\varphi_1^0}$, then at a given $\boldsymbol{\varphi_1^{(k)} = \varphi_1^{(k-1)} + \Delta\varphi_1^{(k)}}$, $\boldsymbol{k = 1 \ldots N}$ are defined:

$$\boldsymbol{\varphi_2^{(k)} = \varphi_2^{(k-1)} + \Delta\varphi_2^{(k)}, \varphi_3^{(k)} = \varphi_3^{(k-1)} + \Delta\varphi_3^{(k)}, \psi^{(k)} = \psi^{(k-1)} + \Delta\psi^{(k)}, k = 1 \ldots N} \tag{15}$$

Here, based on system (7),

$$\Delta\boldsymbol{\varphi_2^{(k)}} = \frac{\Delta\boldsymbol{\varphi_1^{(k)}}}{[A]_{det}} \boldsymbol{l_3 l_1} \left[\begin{array}{c} \boldsymbol{l_{BC} \sin\varphi_3^{(k-1)} \sin\left(\psi^{(k-1)} + \alpha_6 - \varphi_1^{(k-1)}\right) +} \\ \boldsymbol{+ l_6 \sin\psi^{(k-1)} \sin\left(\varphi_3^{(k-1)} - \varphi_1^{(k-1)}\right)} \end{array} \right]$$

$$\Delta\boldsymbol{\psi^{(k)}} = \frac{\Delta\boldsymbol{\varphi_1^{(k)}}}{[A]_{det}} \boldsymbol{l_3 l_2 l_1 \sin\varphi_3^{(k-1)} \sin\left(\varphi_2^{(k-1)} - \varphi_1^{(k-1)}\right)} \tag{16}$$

$$\Delta\boldsymbol{\varphi_3^{(k)}} = \frac{\Delta\boldsymbol{\varphi_1^{(k)}}}{[A]_{det}} \boldsymbol{l_6 l_2 l_1 \sin\psi^{(k-1)} \sin\left(\varphi_2^{(k-1)} - \varphi_1^{(k-1)}\right), k = 1 \ldots N.}$$

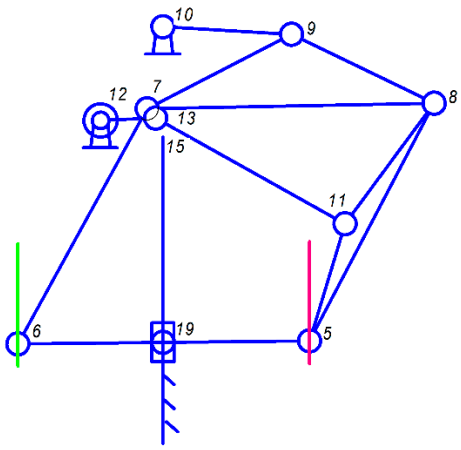
the stroke of the slider is determined by the following formula:

$$\boldsymbol{S^{(k)} = -l_6 \sin\psi^{(k)} + l_3 \sin\varphi_3^{(k)} + d, k = 1 \ldots N} \tag{17}$$

Formulas for calculating the speeds and accelerations of the links and hinges are not given due to the limitation of the volume of the article. They are obtained in a known way by differentiating a system of Equations (3) and (13).

With the help of the above explicit formulas, a general algorithm for the kinematic analysis of the eight-link mechanism on the numerical Maple platform has been compiled. The simulation results are given below.

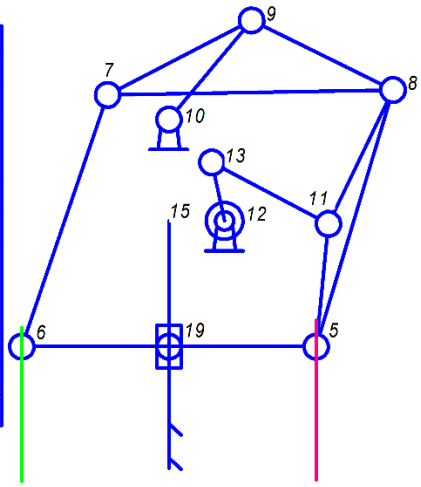
Information about the mechanism			
X9	1,17	Y9	126,59
X10	6,44	Y10	-65,87
X11	5,45	Y11	123,88
X12	6,13	Y12	-6,69
L6-7	158,19	L5-8	159,38
L7-8	171,46	L7-9	97,27
L8-9	94,31	L9-10	77,22
L8-11	89,70	L5-11	72,21
L12-13	32,66	L11-13	129,42
L14-15	189,75	L5-6	174,54
L6-19	87,24	L5-19	87,29
L10-12	66,76	L10-13	53,57



(**a**)

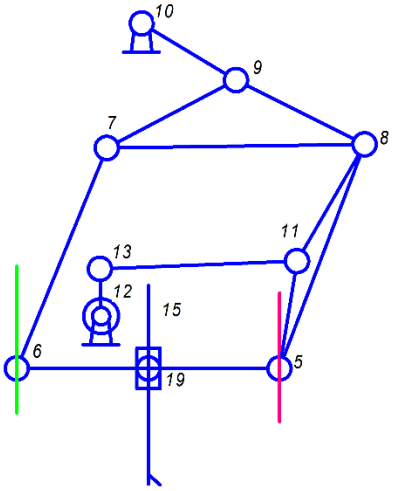
Figure 3. *Cont.*

Information about the mechanism			
X9	30,42	Y9	153,82
X10	6,44	Y10	-65,87
X11	5,45	Y11	123,88
X12	5,86	Y12	44,98
L6-7	158,19	L5-8	159,38
L7-8	171,46	L7-9	97,27
L8-9	94,31	L9-10	77,22
L8-11	89,70	L5-11	72,21
L12-13	35,39	L11-13	79,10
L14-15	189,75	L5-6	174,54
L6-19	87,24	L5-19	87,29
L10-12	69,14	L10-13	35,99



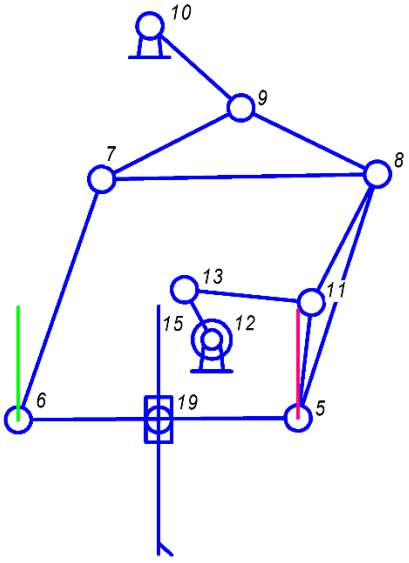
(**b**)

Information about the mechanism			
X9	-22,28	Y9	150,56
X10	6,44	Y10	-65,87
X11	5,45	Y11	123,88
X12	5,66	Y12	84,36
L6-7	158,19	L5-8	159,38
L7-8	171,46	L7-9	97,27
L8-9	94,31	L9-10	76,08
L8-11	89,70	L5-11	72,21
L12-13	31,49	L11-13	131,57
L14-15	189,75	L5-6	174,54
L6-19	87,24	L5-19	87,29
L10-12	198,64	L10-13	165,61



(**c**)

Information about the mechanism			
X9	22,69	Y9	150,80
X10	6,44	Y10	-65,87
X11	5,45	Y11	123,88
X12	5,73	Y12	70,36
L6-7	158,19	L5-8	159,38
L7-8	171,46	L7-9	97,27
L8-9	94,31	L9-10	76,08
L8-11	89,70	L5-11	72,21
L12-13	35,39	L11-13	79,10
L14-15	189,75	L5-6	174,54
L6-19	87,24	L5-19	87,29
L10-12	198,35	L10-13	164,76



(**d**)

Figure 3. Assemblies of knee press mechanisms (18), corresponding to four types of its structure (**a**–**d**).

5. Numerical Experiment and Discussion of Results

Based on the above algorithm, a program for numerical modeling of the kinematic analysis of the mechanism has been comprised. It is assumed that link 1 (crank) performs full rotation, and link 3 (rocker) performs a hobbing motion. Four types of mechanisms of the given structure of the knee press were considered (Figure 1):

$$\begin{array}{l}\text{(a) link 3 performs a hobbing motion at } y_P \geq y_Q \text{and } x_Q = -e;\\ \text{(b) link 3 performs a hobbing motion at } y_P \geq y_Q \text{ and } x_Q = e;\\ \text{(c) link 3 performs a hobbing motion at } y_P \leq y_Q \text{ and } x_Q = -e;\\ \text{(d) link 3 performs a hobbing motion at } y_P \leq y_Q \text{ and } x_Q = e.\end{array} \quad (18)$$

At the same time, the values of the following links of the driven chain of the mechanism will remain unchanged: $l_1 = 32.66$ mm, $l_{BC} = 89.7$ mm, $l_{FP} = l_{CP} = 94.31$ mm, $l_3 = 77.22$ mm, $l_5 = l_6 = 159.38$ mm, $l_{ED} = l_{CF} = 171.46$ mm, $e = 30$ mm. Remaining parameters: l_2, h—take different values for the corresponding types of the mechanism (Figure 2).

Figure 4 shows the results of the kinematic analysis of the first type of the knee press mechanism. The varying parameters are equal: $l_2 = 129.92$ mm, $h = 59.18$ mm. The angular velocity of the input link is equal $\omega_1 = 0.5\ \frac{1}{s}$, then the time of one cycle is $T = 12.56$ s. The slider stroke is $S_1 = 74$ mm. Output link 7 (slider) remains stationary for a long time. $t_{b1} = 4.2$ s, i.e., the slider performs almost one third of the working cycle. Figure 4a,b shows graphs of the velocity and acceleration of the interrelationship with the graph of the position function. By definition, dwell occurs when one or more consecutive derivatives of the position functions of the output link simultaneously vanishes. From Figure 4b, it can be seen that during dwell, the velocity and acceleration remain close to zero.

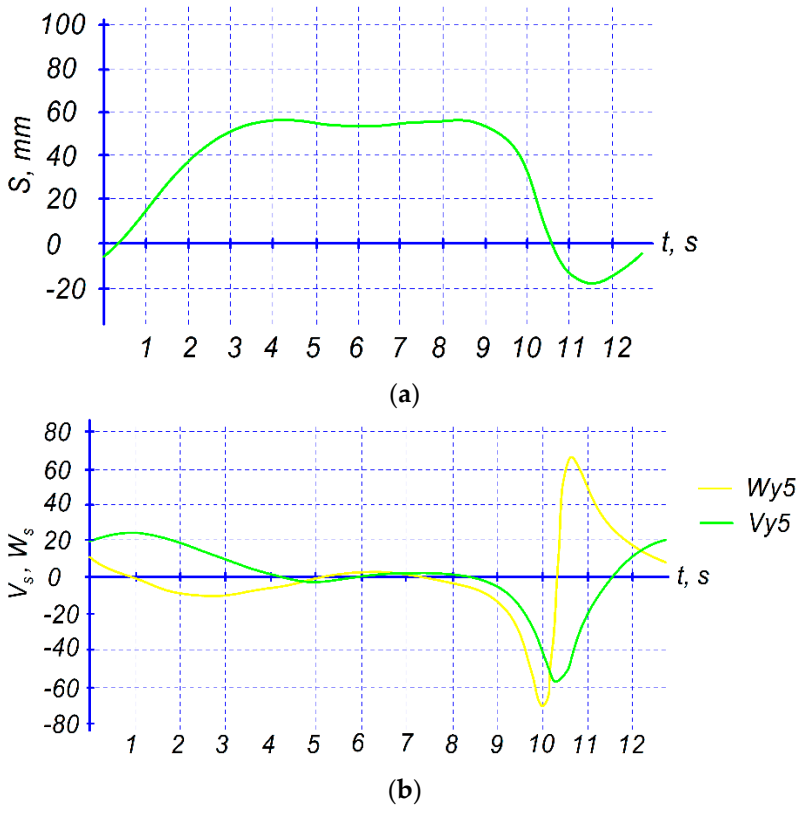


Figure 4. Results of the kinematic analysis of the first type of the knee press mechanism: (**a**) graph of the function of the position output link (slider); (**b**) graphs of the speed and acceleration of the slider.

Figure 5 shows the results of the kinematic analysis of the second type of knee press mechanism. The variable parameters are equal: $l_2 = 79.1$ mm, $h = 59.18$ mm. In this case, the slider stroke is $S_2 = 97$ mm $> S_1$. The output link 7 (slider) remains motionless $t_{b2} = 2.5$ s. Figure 5b. At the same time, the slider 7 performs fast working stroke $S_2 = 97$ mm in $t_{motion} = 0.34$ s and the acceleration changes rapidly within $w_7 \in [-600, 400] \frac{mm}{s^2}$; that is, there is a blow.

In the considered options, when $y_P \geq y_Q$, there is a slider dwell in its upper position. At the same time, the slider dwell $t_{b1} = 4.2$ s at $x_Q = -e$ significantly more than the dwell $t_{b2} = 2.5$ s at $x_Q = e$.

Figure 6 shows the results of the kinematic analysis of the third option of the knee press mechanism. The variable parameters are equal: $l_2 = 131.57$ mm, $h = 150.23$ mm. In this case, the dwell of the working slider occurs in the lower position when there is direct contact with the workpiece and the slider stroke is $S_3 = 100$ mm. The output link 7 (slider) remains stationary $t_{b3} = 4.04$ s. Figure 6a amounts to 1/3 T—total working cycle time. In some crank presses, there are requirements when it is necessary to ensure rapid compression of the forging and a long reverse of the slide stroke [4,22]. Such a process can be provided by this structure of the crank press mechanism. In Figure 6a it can be seen that the forging compression time $t_{co} = 2.7$ s, and reverse time $t_{co} = 5.8$ s. From Figure 6b it can be seen that during the dwell, the velocity and acceleration remain close to zero.

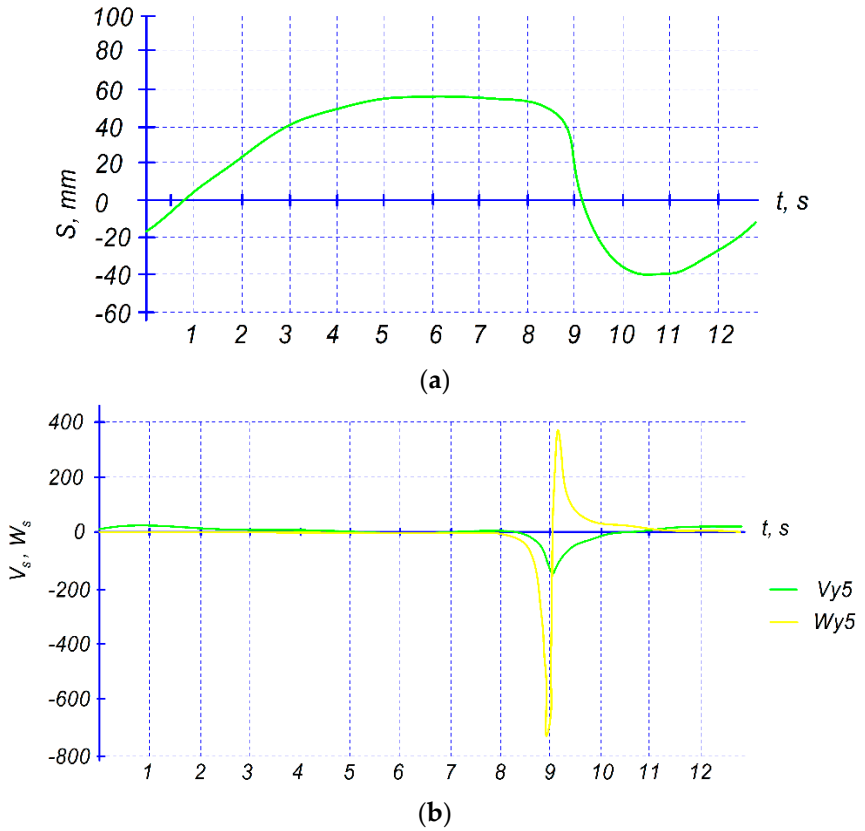


Figure 5. Results of the kinematic analysis of the second type of the knee press mechanism: (**a**) graph of the function of the position of the output link (slider); (**b**) graphs of the position, speed, and acceleration of the slider.

Figure 7 shows the results of the kinematic analysis of the fourth option of the knee press mechanism. The variable parameters are equal: $l_2 = 79.1$ mm, $h = 136.23$ mm. In this case, the dwell of the working slider also occurs in the lower position and the slider stroke is $S_4 = 102$ mm, which is the same with the dwell of the working link in the third option. The output link 7 (slider) remains stationary, $t_{b4} = 2.08$ s $< t_{b3}$; Figure 7a, which represents 1/6 T—total working cycle time. This version of the mechanism also provides

rapid compression of the forging and a long reverse motion. In Figure 6a it can be seen that the forging compression time is $t_{co} = 3.06$ s, and reverse motion time $t_{co} = 7.4$ s. From Figure 7b it can be seen during the dwell that the velocity and acceleration remain close to zero, i.e., there is an approximate working link dwell.

Figure 8 shows the results of a kinematic analysis of the third option of the knee press mechanism by the angular positions of the links. From the analysis of the graphs, it can be seen that the triangular link 4 makes a translational movement since the angular coordinate is constant. The angular coordinates of links 5 and 6 (pink) and link 2 (orange) change. The angular coordinate of crank 1 is marked in yellow. Similarly, the angular coordinates of the links of the mechanisms in other versions of the crank press change.

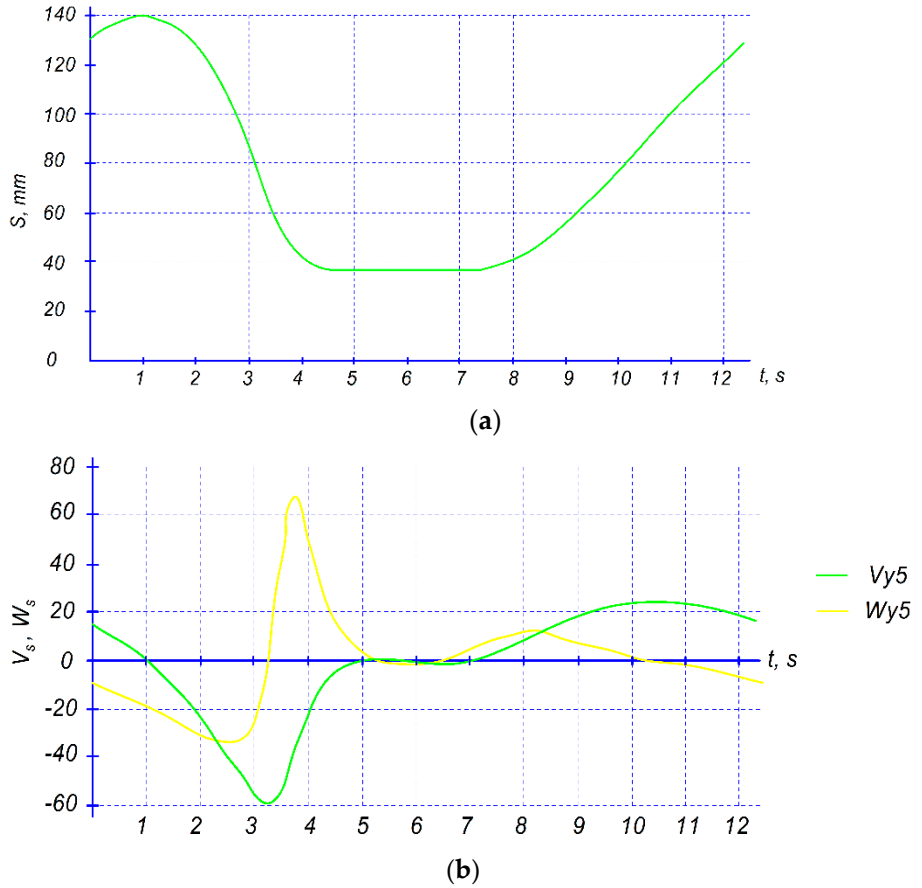


Figure 6. Results of the kinematic analysis of the third option of the knee press mechanism: (**a**) graph of the function of the position of the output link (slider); (**b**) graphs of the position, speed, and acceleration of the slider.

To conduct a comparative analysis of the results obtained, it was also decided to model the mechanism on the Solidworks package, calculations of which, as is known are based on numerical methods such as the finite element method, etc. The movement of the mechanism was modeled on the Solidworks Motion module, which serves for accurate modeling and analysis of motion in the assembly, taking into account the impact of elements of motion research. The coordinates of the hinges were found by numerical solution of a set of related differential and algebraic equations that determine the movement of the model using such well-known methods as GSTIFF, WSTIFF, and SI2_GSTIFF. For the interaction of the elements of the mechanism between the links and the hinges, conjugations of the "concentricity" and "coincidence" types were used. Since the leading element was the OA link, then, accordingly, an external force (Motor) was applied to the OA link. The simulation results are presented below.

Comparison of the results in Figure 9 by the position of the slider (Figure 9a) with the result shown in Figure 5a shows full compliance. This means that the numerical program and algorithm developed on the basis of our methodology are correct.

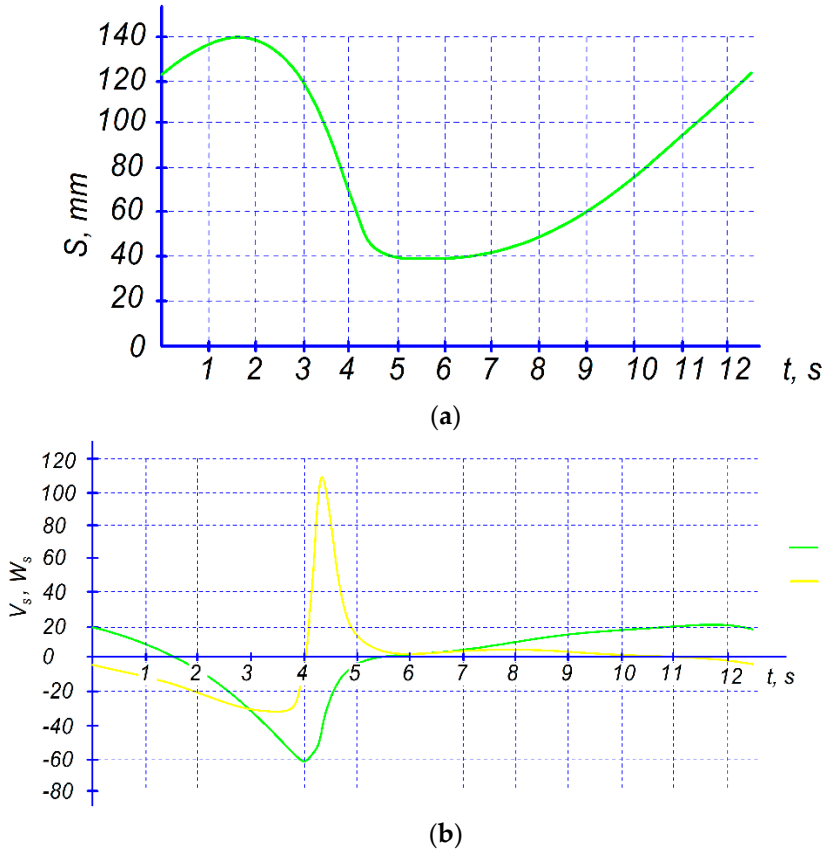


Figure 7. Results of kinematic analysis of the fourth option of the knee press mechanism: (**a**) a graph of the function of the position of the output link (slider); (**b**) graphs of the position, speed, and acceleration of the slider.

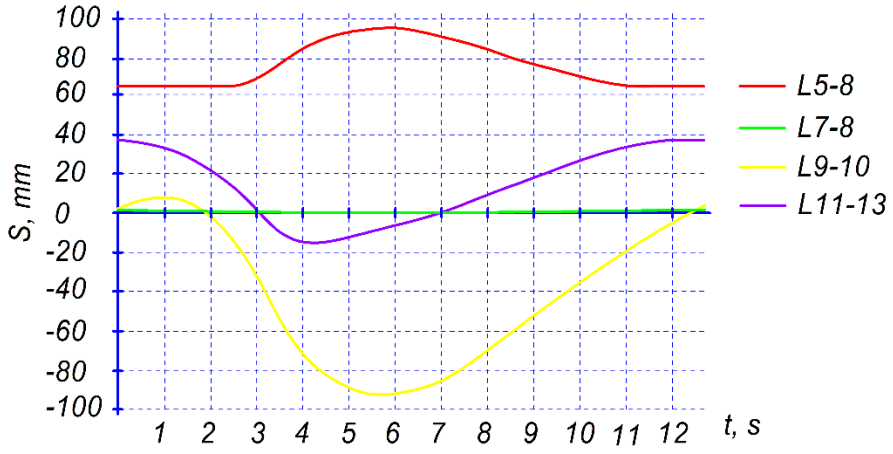
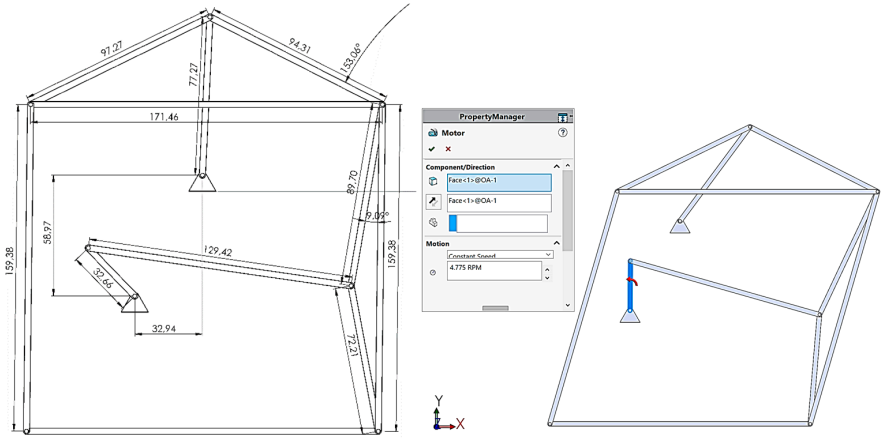
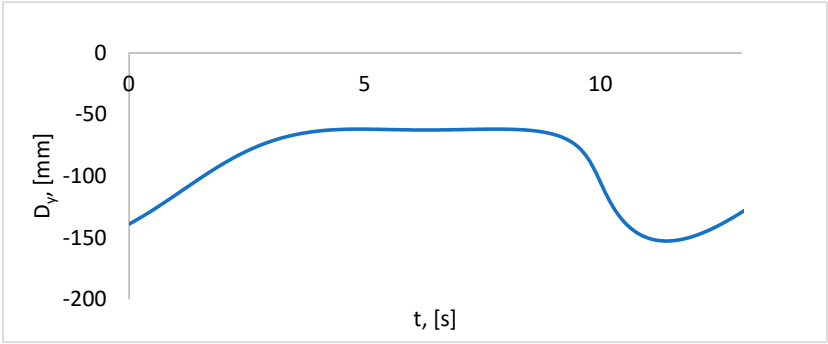


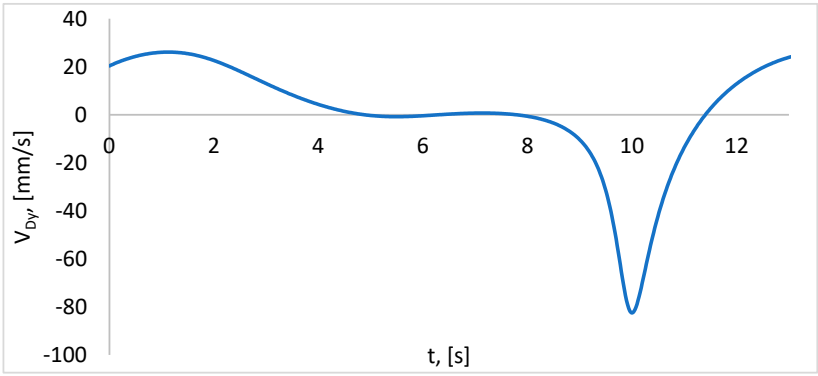
Figure 8. Results of kinematic analysis of the third option of the knee press mechanism by the angular positions of the links.



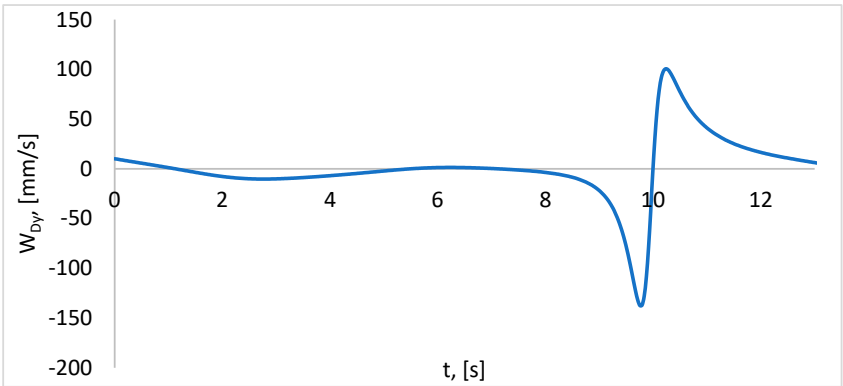
(**a**)



(**b**)



(**c**)



(**d**)

Figure 9. Modeling of the mechanism on the Solidworks platform: (**a**) assembly of the mechanism in the Solidworks environment; (**b**) changing the coordinates of the slider along the *y* axis; (**c**) changing the speed of the slider along the *y* axis; (**d**) changing the acceleration of the slider along the *y* axis.

6. Conclusions

As a result of the research, new designs of eight-link actuators of crank knee presses with an improved configuration and long dwells of the working slider are proposed. A methodology has been developed for studying the kinematics of a high-class eight-link crank-slider mechanism, which is based on the use of methods for replacing the leading link and analyzing small displacements. A numerical explicit algorithm and a kinematics modeling program on the Maple platform have been developed. The possibility of regulating the duration of the slider dwell depending on the eccentricity of the slider guide and the coordinates of the fixed racks is investigated. Based on the numerical experiment and the selection of certain geometric dimensions of four knee press mechanisms with different values of the dwell and of the working slider stroke. They can be taken as initial approximations to solve the problem of precisely synthesizing the knee press mechanism with given values of the stroke and the duration of the dwell of the slider.

Author Contributions: A.T., concept development; B.A., holding research; M.K., holding statistical analysis; B.M., prepared and edited text; G.-G.A.I.; created software. All authors have read and agreed to the published version of the manuscript.

Funding: The work was carried out within the framework of the grant project AP14972874 funded by the Science Committee of the Ministry and Higher Education of the Republic of Kazakhstan.

Institutional Review Board Statement: Not applicable.

Informed Consent Statement: Not applicable.

Data Availability Statement: Data are contained within the article.

Conflicts of Interest: The authors declare no conflict of interest.

References

1. Evgrafov, M.; Semyonov, Y.; Sloushch, A. *Theory of Mechanisms and Machines: Study Guide*; Publishing Center "Academy": Moscow, Russia, 2006; 560p.
2. Bocharov, Y. *Forging and Stamping Equipment*; Publishing Center "Academy": Moscow, Russia, 2008; 480p.
3. Matthews, S.; Tanninen, P.; Toghyani, A.; Eskelinen, H.; Ovaska, S.-S.; Leminen, V.; Varis, J. Novel method for Selection of Drive Motor in Paperboard Forming Press Utilizing Multi-Dynamics Model based on Material Thickness. In *Procedia Manufacturing, Proceedings of the 27th International Conference on Flexible Automation and Intelligent Manufacturing, FAIM2017, Modena, Italy, 27–30 June 2017*; Elsevier: Amsterdam, The Netherlands, 2017; Volume 11, pp. 2091–2098.
4. Chen, Y.; Sun, Y.; Yang, D. Investigations on the dynamic characteristics of a planar slider-crank mechanism for a high-speed press system that considers joint clearance. *J. Mech. Sci. Technol.* **2017**, *31*, 75–85. [CrossRef]
5. Telegin, I.; Shumilova, T. Comparing the efficiency of flowsheets for hot die forging on crank presses. In Proceedings of the MATEC Web of Conferences, Sevastopol, Russia, 10–14 September 2018; Volume 224, p. 01092.
6. Moldabekov, M.; Tuleshov, A.; Ualiev, G. *Mathematical Modeling of the Dynamics of Mechanisms and Machines*; Kazak University: Almaty, Kazakhstan, 1998; 204p.
7. Shihao, L.; Mao, L. *Design and Test of the Crank Slider Mechanism Feeding Type Rubber Rotary Cutting Machine*; Springer Nature: Cham, Switzerland, 2020; Volume 2, p. 917. [CrossRef]
8. Ouyang, P.; Li, Q.; Zhang, W. Design, modelling and control of a hybrid machine. *Mechatronics* **2004**, *14*, 1197–1217. [CrossRef]
9. Yuan, Z.; Gilmartin, M.; Douglas, S. Design of hybrid machines for nonuniform. *Proc. Inst. Mech. Eng. Part C J. Mech. Eng. Sci.* **2005**, *219*, 491–499. [CrossRef]
10. Kutuk, M.; Dulger, L. A hybrid press system: Motion design and inverse kinematics issues. *Eng. Sci. Technol. Int. J.* **2016**, *19*, 846–856.
11. Tuleshov, A.; Jamalov, N.; Jomartov, A. Crank-Slide Mechanism of the Press. Patent of the Republic of Kazakhstan for Invention No. 33874. Applicant and Patent Holder JIME Named after Dzholdasbekov, U.— No. 2018/0225.1, 10 April 2018.
12. Jamalov, N.; Tuleshov, A.; Jomartov, A.; Seidakhmet, A.; Kamal, A. Crank-Knee Press Mechanism. Eurasian Patent for Invention No. 038760; Applicant and Patent Holder of the Dzholdasbekov U. JIME, 15 October 2021.
13. Tuleshov, A.; Halicioglu, R.; Shadymanova, A.; Kuatova, M. Kinematic synthesis method and eccentricity effects of a Stephenson mechanism. *Mech. Sci.* **2021**, *12*, 1–8. [CrossRef]
14. Connor, A.; Douglas, S.; Gilmartin, M. The synthesis of hybrid five-bar path generating mechanisms using genetic algorithms. In Proceedings of the 1st International Conference on Genetic Algorithms in Engineering Systems: Innovations and Applications, Sheffield, UK, 12–14 September 1995; pp. 313–318.

15. Dülger, L.; Kireçci, A.; Topalbekiroglu, M. Modeling and simulation of a hybrid actuator. *Mech. Mach. Theory* **2003**, *38*, 395–407. [CrossRef]
16. Yu, H. Modeling and control of hybrid machine systems—A five-bar mechanism case. *Int. J. Autom. Comput.* **2006**, *3*, 235–243. [CrossRef]
17. Li, H.; Zhang, Y. Seven bar mechanical press with hybrid driven mechanism for deep drawing; part 1: Kinematics analysis and optimum design. *J. Mech. Sci. Technol.* **2010**, *24*, 2153–2160. [CrossRef]
18. Li, H.; Tso, P.L. Experimental study on a hybrid driven press using iterative learning control. *Int. J. Mach. Tools Manuf.* **2008**, *48*, 209–219. [CrossRef]
19. Tso, P.L. Optimal Design of a Hybrid-Driven Servo Press and Experimental Verification. *J. Mech. Des.* **2010**, *132*, 034503. [CrossRef]
20. Yan, H.S.; Chen, W.R. A variable input speed approach for improving the output motion characteristics of Watt-type presses. *Int. J. Mach. Tools Manuf.* **2000**, *40*, 675–690. [CrossRef]
21. Halicioglu, R.; Jomartov, A.; Kuatova, M. Optimum Design and Analysis of a Novel Planar Eight-Bar Linkage Mechanism. *Mech. Based Des. Struct. Mach.* **2021**, *51*, 5231–5252. [CrossRef]
22. Tuleshov, A.; Drakunov, Y.; Jomartov, A.; Seidakhmet, A.; Jamalov, N.; Tuleshov, E.; Kuatova, M. *Crank Lever Presses Based on the Stephenson Mechanism II: Monograph*; JIME: Almaty, Kazakhstan, 2020; 240p, ISBN 978-601-332-973-4.

Disclaimer/Publisher's Note: The statements, opinions and data contained in all publications are solely those of the individual author(s) and contributor(s) and not of MDPI and/or the editor(s). MDPI and/or the editor(s) disclaim responsibility for any injury to people or property resulting from any ideas, methods, instructions or products referred to in the content.